Optofluidic trapping and transport on solid core waveguides within a microfluidic device

Bradley S. Schmidt[1], Allen H. J. Yang[2], David Erickson[3], and Michal Lipson[1]

[1]*School of Electrical and Computer Engineering, Cornell University, Ithaca, NY 14853*
[2]*School of Chemical and Biomolecular Engineering, Cornell University, Ithaca, NY 14853*
[3]*Sibley School of Mechanical and Aerospace Engineering, Cornell University, Ithaca, NY 14853*
lipson@ece.cornell.edu; de54@cornell.edu

Abstract: In this work we demonstrate an integrated microfluidic/photonic architecture for performing dynamic optofluidic trapping and transport of particles in the evanescent field of solid core waveguides. Our architecture consists of SU-8 polymer waveguides combined with soft lithography defined poly(dimethylsiloxane) (PDMS) microfluidic channels. The forces exerted by the evanescent field result in both the attraction of particles to the waveguide surface and propulsion in the direction of optical propagation both perpendicular and opposite to the direction of pressure-driven flow. Velocities as high as 28 μm/s were achieved for 3 μm diameter polystyrene spheres with an estimated 53.5 mW of guided optical power at the trapping location. The particle-size dependence of the optical forces in such devices is also characterized.

OCIS codes: (130.3120) Integrated optics devices; (230.7370) Waveguides; (140.7010) Trapping.

References and links

1. H. A. Stone, A. D. Stroock, and A. Ajdari, "Engineering flows in small devices: microfluidics toward a lab-on-a-chip," Annu. Rev. Fluid Mech. **36**, 381–411 (2004).
2. A. Ashkin, J. M. Dziedzic, J. E. Bjorkholm, and S. Chu, "Observation of a single-beam gradient force optical trap for dielectric particles," Opt. Lett. **11**, 288-290 (1986).
3. D. G. Grier, "A revolution in optical manipulation," Nature **424**, 810-816 (2003).
4. K. C. Neuman and Steven Block, "Optical trapping," Rev. Sci. Instrum. **75**, 2787-2809 (2004).
5. P. J. Rodrigo, V. R. Daria, and J. Glückstad, "Real-time three-dimensional optical micromanipulation of multiple particles and living cells," Opt. Lett. **29**, 2270-2272 (2004).
6. M. P. MacDonald, G. C. Spalding, and K. Dholakia, "Microfluidic sorting in an optical lattice," Nature **426**, 421-424 (2003).
7. R. Applegate, Jr., J. Squier, T. Vestad, J. Oakey, and D. Marr, "Optical trapping, manipulation, and sorting of cells and colloids in microfluidic systems with diode laser bars," Opt. Express **12**, 4390-4398 (2004).
8. F. Merenda, J. Rohner, J. -M. Fournier, and R.-P. Salathé, "Miniaturized high-NA focusing-mirror multiple optical tweezers," Opt. Express **15**, 6075-6086 (2007).
9. F. Arai, A. Ichikawa, M. Ogawa, T. Fukuda, K. Horio, and K. Itoigawa, "High-speed separation of randomly suspended single living cells by laser trap and dielectrophoresis," Electrophoresis **22**, 283-288 (2001).
10. F. V. Ignatovich and L. Novotny, "Experimental study of nanoparticle detection by optical gradient forces," Rev. Sci. Instrum. **74**, 5231-5235 (2003).
11. M. Ozkan, M. Wang, C. Ozkan, R. Flynn, and S. Esener, "Optical manipulation of objects and biological cells in microfluidic devices," Biomed. Microdevices **5**, 61-67 (2003).
12. J. Enger, M. Goksor, K. Ramser, P. Hagberg, and D. Hanstorp, "Optical tweezers applied to a microfluidic system," Lab. Chip **4**, 196-200 (2004).
13. S. Tan, H. A. Lopez, C. W. Cai, and Y. Zhang, "Optical trapping of single-walled carbon nanotubes," Nano Lett. **4**, 1415-1419 (2004).
14. S. Cran-McGreehin, T. F. Krauss and K. Dholakia, "Integrated monolithic optical manipulation," Lab Chip **6**, 1122-1124 (2006).

#86071 - $15.00 USD Received 6 Aug 2007; revised 25 Sep 2007; accepted 27 Sep 2007; published 15 Oct 2007

15. E. Almaas and I. Brevik, "Radiation forces on a micrometer-sized sphere in an evanescent field," J. Opt. Soc. Am. B **12**, 2429-2438 (1995).
16. M. Lester and M. Nieto-Vesperinas, "Optical forces on microparticles in an evanescent laser field," Opt. Lett. **24**, 936-938 (1999).
17. H. Y. Jaising and O. G. Hellesø, "Radiation forces on a Mie particle in the evanescent field of an optical waveguide," Opt. Commun. **246**, 373-383 (2005).
18. A. Rahmani and P. C. Chaumet, "Optical trapping near a photonic crystal," Opt. Express **14**, 6353-6358 (2006).
19. S. Mandal and D. Erickson, "Optofluidic transport in liquid core waveguiding structures," Appl. Phys. Lett. **90**, 184103 (2007).
20. S. Kawata and T. Tani, "Optically driven Mie particles in an evanescent field along a channeled waveguide," Opt. Lett. **21**, 1768-1770 (1996).
21. T. Tanaka and S. Yamamoto, "Optically induced propulsion of small particles in an evanescent field of higher propagation mode in a multimode, channeled waveguide," Appl. Phys. Lett. **77**, 3131-3133 (2000).
22. K. Grujic, O. G. Hellesø, J. P. Hole, and J. S. Wilkinson, "Sorting of polystyrene microspheres using a Y-branched optical waveguide," Opt. Express **13**, 1-7 (2005).
23. K. Grujic and O. G. Hellesø, "Dielectric microsphere manipulation and chain assembly by counter-propagating waves in a channel waveguide," Opt. Express **15**, 6470-6477 (2007).
24. S. Gaugiran, S. Gétin, G. Colas, A. Fuchs, F. Chatelain, J. Dérouard, and J.M. Fedeli, "Optical manipulation of microparticles and cells on silicon nitride waveguides," Opt. Express **13**, 6956-6963 (2005).
25. D. Psaltis, S.R. Quake, and C. Yang, "Developing optofluidic technology through the fusion of microfluidics and optics," Nature **442**, 381-386 (2006).
26. C. Monat, P. Domachuk, and B. J. Eggleton, "Integrated optofluidics: A new river of light," Nature Photonics **1**, 106-114 (2007).
27. B. Beche, N. Pelletier, E. Gaviot, and J. Zyss, "Single-mode TE_{00}-TM_{00} optical waveguides on SU-8 polymer," Opt. Commun. **230**, 91-94 (2004).
28. B. Y. Shew, C. H. Huo, Y. C. Huang, Y. H. Tsai, "UV-LIGA interferometer biosensor based on the SU-8 optical waveguide," Sens. Actuators A **120**, 383-389 (2005).
29. D. Esinenco, S. D. Psoma, M. Kusko, A. Schneider, and R. Muller, "SU-8 micro-biosensor based on Mach-Zender interferometer," Rev. Adv. Mater. Sci. **10**, 295-299 (2005).
30. MicroChem, http://www.microchem.com
31. D. C. Duffy, J. C. McDonald, O. J. A. Schueller, and G. M. Whitesides, "Rapid prototyping of microfluidic systems in poly(dimethylsiloxane)," Anal. Chem. **70**, 4974-4984 (1998).
32. Duke Scientific Corporation, http://www.dukescientfic.com
33. A. H. J. Yang and D. Erickson "Stability analysis of optofluidic transport on solid-core waveguiding structures" Submitted (2007).
34. L. N. Ng, B. J. Luff, M. N. Zervas, and J. S. Wilkinson, "Forces on a Rayleigh particle in the cover region of a planarwaveguide," Lightwave Tech. Lett. **18**, 388-400 (2000).
35. J. Happel and H. Brenner, *Low Reynolds Number Hydrodynamics, with Special Applications to Particulate Media* (Noordhoff International, 1973).

1. Introduction

Within microfluidic systems, optical forces represent an additional form of particle transport that complements traditional manipulation techniques such as pressure driven flow and electro-kinetics [1]. To date, the most well exploited use of optical forces [2-5] in such microfluidic devices has been the ability to sort microscale objects based on properties such as size, refractive index, absorption, and dispersion. Examples of such works include the sorting of particles using various 3-D optical lattices [6], laser diode bars [7], micro-mirrors [8], and single beam free space trapping [9-13], all involving the combination of microfluidics and optical trapping, but without the additional advantages provided by the use of waveguiding structures. Interested readers are also referred to the recent work by Cran-McGreehin et al. [14] who present an integrated monolithic architecture for on-chip optical manipulation.

Evanescent field-based optical transport and trapping [15-17] using photonic structures has several advantages over free-space systems. Analogous to the advantages seen for telecom and datacom applications, the use of planar photonic structures in microfluidic devices removes the need for table-top free-space optics, potentially reducing costs and

#86071 - $15.00 USD Received 6 Aug 2007; revised 25 Sep 2007; accepted 27 Sep 2007; published 15 Oct 2007

increasing platform portability. A more fundamental consideration is that in free-space systems, the impulse applied to a particle is limited by the focal depth of the objective lens and the manipulation area is limited by the spot size of the laser. With waveguides the optical forces can be applied over long distances, limited only by the scattering and absorption losses in the system. In addition, the nature of lithographic methods used to produce planar photonic devices allows for the creation of thousands of parallel systems on the same substrate so that many trapping processes can be performed simultaneously over a large area. Another advantage of using high refractive–index-contrast materials is that they allow for controlled distribution of the optical energy over dimensions much smaller than the free-space wavelength of light. Finally, photonic structures give access to a new class of subtle design parameters that can be exploited, including waveguide cross-sectional dimensions, polarization sensitivities, bends, and wavelength-specific devices such as couplers and field-enhancing microcavities [18]. In comparison the free space systems described above and recently demonstrated liquid core optofluidic transport systems [19], such systems are limited by the total amount of energy available in the evanescent field and the requirement that particles must first be brought into the waveguide near-field in order to be transported. The former of these disadvantages is offset by the higher intensity available from the more strongly confined mode and the longer interaction lengths.

In this work we demonstrate an optical trapping platform based on planar waveguides that are integrated with microfluidic channels. Previous efforts using evanescent fields for optical trapping have shown propulsion of dielectric particles along waveguides [20] including waveguides made of ion-exchange doped glasses [21-23] and silicon nitride waveguides [24] within static fluid cells. Extending these previous works, we demonstrate here: (1) the use of the evanescent field surrounding a waveguide to directly capture and transport dielectric particles initially carried within a pressure driven flow in a microfluidic system, (2) the capture and stable transport of particles both perpendicular and opposite to an imposed pressure driven flow along both straight and curved waveguides and (3) the chromatographic and fractionation properties of the system through characterization of the size dependence on transport velocity using both numerical and experimental means. The optofluidic [25,26] platform developed here is comprised of SU-8 epoxy-based photonic structures, combined with poly(dimethylsiloxane) (PDMS) microfluidics on a fused silica substrate. This combination allows for the creation of a simple yet functional optical manipulation system for lab-on-chip applications.

2. Optofluidic platform design and fabrication

In this work our waveguiding structures are fabricated from SU-8, an epoxy-based negative UV photoresist that is strongly chemical-resistant after processing. The mechanical hardness and chemical resistance of SU-8 make it an excellent material for use in lab-on-chip analysis systems. It is also an excellent lightguiding material [27-29] with high transparency in the wavelength range of interest (850-1100 nm), since these wavelengths have very low absorption for water and many biological materials of possible interest. The fused silica substrate has a refractive index of 1.453, while the exposed SU-8 film has a measured refractive index of 1.554 at λ=975 nm, which along with the water cladding with refractive index of 1.33 provides for significant refractive-index contrast for high confinement and strong evanescent field gradients. The waveguide dimensions were chosen to be a height of 560 nm and a width of 2.8 μm. A custom, full vector, finite-difference, mode-solver simulation was employed to numerically calculate the cross-sectional electric field distribution for the fundamental quasi-TM mode as shown below in Fig. 1.

#86071 - $15.00 USD Received 6 Aug 2007; revised 25 Sep 2007; accepted 27 Sep 2007; published 15 Oct 2007

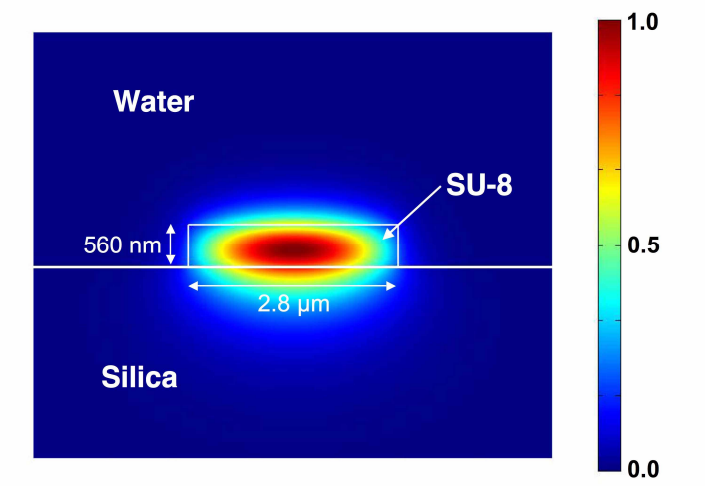

Fig. 1. The electric field profile of the quasi-TM mode for a water-clad SU-8 waveguide on a fused silica substrate. The waveguide height and width are 560 nm and 2.8 μm respectively.

The TM mode is of greater interest than the TE mode for this waveguide, as there exists a stronger discontinuity of the field on the top surface of the waveguide due to the significant contrast between the refractive indices at this interface, which creates stronger gradients critical for the particle to be trapped and propelled.

The waveguides were fabricated using standard photolithographic techniques. The SU-8 resist with MicroChem formulation 2000.5 [30] was spun at 2000 rpm for 40 seconds to form a film thickness of 560 nm. The film was baked at 65°C for 2 minutes, then at 95°C for 2 minutes, and then the waveguide pattern was exposed with a g-line (λ=436 nm) 5x stepper. A post-exposure bake was performed, again at 65°C and 95°C for 2 minutes at each temperature. The sample was developed using SU-8 developer solution for 60 seconds, rinsed and dried. The input and output facets of the waveguides were diced from the backside with a dicing saw to a distance of only 50 microns from the top surface and then cleaved by applying simple pressure to the substrate by hand.

The microfluidics were made using a standard procedure for creating PDMS microfluidics by solution-casting using a lithographically patterned mold [31]. The channels were designed to dimensions of 5 μm in height and 100 μm wide. We used relatively shallow channels to confine the flowing particles as close as possible to the waveguides. The PDMS channels and the waveguide sample were both plasma-cleaned for several seconds and then bonded by pressure following alignment in a contact aligner. The channels were aligned perpendicularly to the waveguide inputs with approximately 600 microns of exposed waveguide from the facet of the chip to the edge of the PDMS on both the input and output side of the chip and approximately 2.7 mm from the edge of the chip to the fluidic channel. Finite-Difference-Time-Domain (FDTD) simulations confirm that the expected losses due to the change of cladding from air to PDMS and PDMS to water in the channel are less than 2.7% and 0.9% respectively. The same waveguide is asymmetric when it is air-clad, therefore it supports only one TM mode and therefore acts as a filter so that only the fundamental TM mode will propagate into the PDMS-clad water-clad sections of the waveguides.

3. Experimental setup

The light source used for testing was a fiber coupled laser diode module with a wavelength of λ=975 nm which was fiber that was connected to an isolator to protect the laser from back reflections. A polarization controller was also used along with a 99%-1% tap to measure the

#86071 - $15.00 USD Received 6 Aug 2007; revised 25 Sep 2007; accepted 27 Sep 2007; published 15 Oct 2007

input power that was then coupled to a lensed fiber. This lensed fiber was used to couple light into the waveguides, and the output light was collected with an objective lens and measured with a detector. The lensed fiber was not itself polarization maintaining however a polarization controller was used to select the TM-like polarization and a polarization filter was placed between the objective lens and the detector at the output to ensure the measurement of the correct polarization. The PDMS fluidic layer was bonded at a distance of 600 μm from the edge of the chip to allow clear imaging of the fiber-to-waveguide alignment, as well as to ensure that the air-clad structure, which is single-mode for the TM polarization, would prevent the excitation of second order modes in the slightly-multimode PDMS clad waveguide. As mentioned in section 2, our numerical simulations predicted stronger trapping fields for the TM polarization. This was qualitatively confirmed in the experiments outlined below (in that we observed more stable trapping in TM mode than TE) however the effects of polarization on trapping stability are not fully characterized here.

The particles used in our experiment were polystyrene spheres with refractive index n=1.574 at λ=975 nm [32] of various sizes at concentrations between 0.1-0.2 g/L in a 100 mM phosphate buffer solution (PBS) with a regulated pH of 7.0. The reason for increasing the ionic concentration over DI water is to reduce electrostatic interactions in the system. The spheres contained fluorescent dyes so that they could be imaged more clearly and to distinguish among different sized particles within the same channel. An upright microscope with a CCD camera was used to track the particles' movements within the channel.

4. Experimental demonstration of trapping in the presence of a pressure driven cross flow.

In our experimental system, as shown in Fig. 2 below, dielectric particles are convected along with the pressure driven flow in the main microfluidic channel. When a particle comes in contact with the optically excited waveguide it may be captured in the evanescent field and begin moving in the direction of optical propagation. This trapping exhibited a dependence on pressure driven flow speed and the waveguide optical power. In particular, a greater portion of the particles are captured at lower flow speeds and higher optical powers. Though not yet fully characterized, we expect that this is a result of slower particles having less momentum to overcome the attraction well of the evanescent field and the higher power increasing the trapping stability [33]. Using the system described here we observed particle trapping and optical transport velocities along the waveguide as high as 30 μm/sec. In what follows, we use the term "flow velocity" to indicate the average velocity of the particle in the pressure driven flow and "optical transport velocity" to indicate the net velocity of the particle along the waveguide.

#86071 - $15.00 USD Received 6 Aug 2007; revised 25 Sep 2007; accepted 27 Sep 2007; published 15 Oct 2007

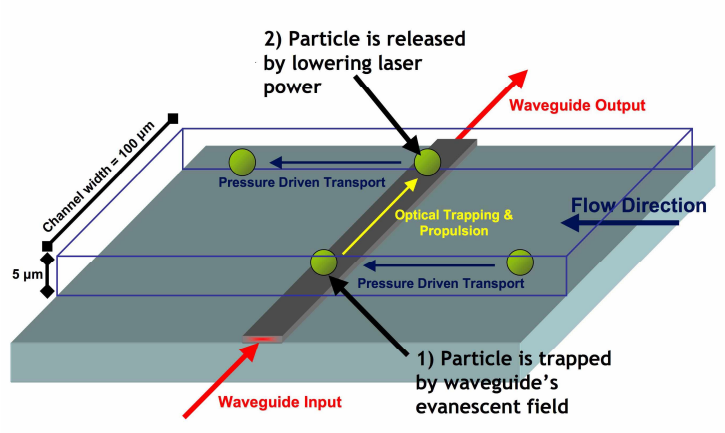

Fig. 2. Schematic of trapping experiment. The optical waveguide propulsion is perpendicular to the direction of the pressure driven flow in the channel.

The trapping of several particles is shown in Fig. 3. Due to the drag on the particle in the solution, the particles quickly reach a terminal optical transport velocity. Occasionally, particles were knocked off the waveguide likely due to fluctuations in the fluid flow or physical irregularities in the waveguide, but most often they were transported to the wall of the channel and remained held until the trapping force was reduced by lowering the input power.

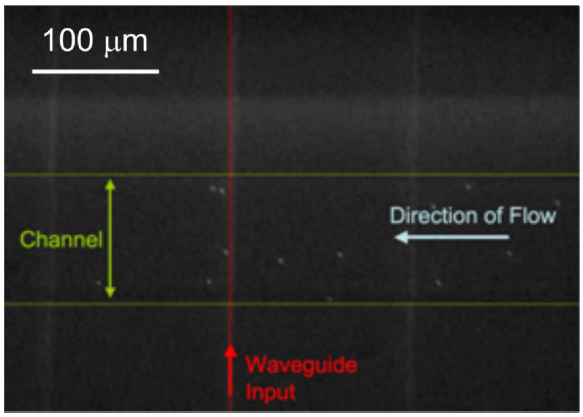

Fig. 3. (124 kB) Movie of the propulsion of particles with a diameter of 2 µm.

The optical power in the waveguide at the channel location is calculated by estimating the losses of the waveguides and bends. These numbers were extracted using varying lengths of waveguides and numbers of bends to determine the coupling losses from the fiber into the air-clad waveguide and then into the PDMS-clad waveguide, the bending losses, and the waveguide propagation losses. The losses in the waveguides were measured to be 1.3 ± .2 dB/cm, while the input coupling loss was measured to be 5.0 ± .2 dB. With these measured losses a guided power of 10 mW in the channel corresponds to an output from the lensed fiber of 35.5 mW. The linear relationship between optical transport velocity of a given size of particle and the guided power is shown in Fig. 4 below for a series of 3 µm diameter particles.

#86071 - $15.00 USD Received 6 Aug 2007; revised 25 Sep 2007; accepted 27 Sep 2007; published 15 Oct 2007

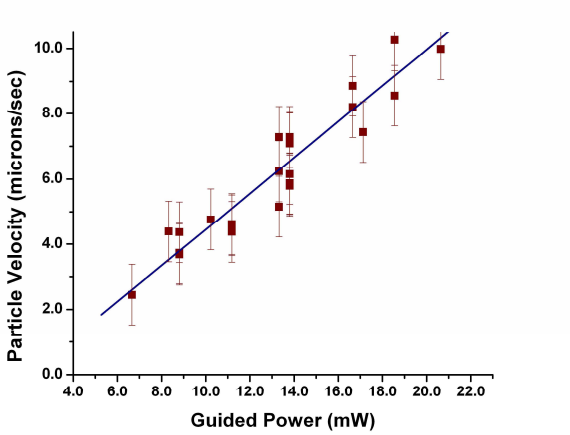

Fig. 4. Plot of terminal optical transport velocity vs output power for a series of 3 μm diameter particles on the same waveguide. Optical transport velocities measured perpendicular to the direction of the imposed pressure driven flow and therefore represent only the effects of optical propulsion. Each data point represents average velocity of a single particle trapped on a waveguide. Error bars represent standard deviation of velocity measurements for the given particle (i.e. for each trapped particle multiple velocity measurements were made at different points on the waveguide).

The variability in the results is partially due to the variation of particle size as specified by the manufacturer (~5%). Higher peak optical transport velocities of 28 μm/s were achieved using guided powers of 53.5 mW for 3 μm diameter spheres, but operating at currents beyond the normal range of the relatively weak diode laser. Gradient trapping to pull the spheres from the flows to the waveguide was achieved at guided powers as low as 6.8 mW, at which point fluctuations in the flow made stable trapping difficult.

5. Calculation of optical propulsion force and particle terminal velocity

In free-space, the forces on a small, trapped particle are often approximated by an attractive gradient force that is due to a strong gradient of the field near the focus of a beam, and a scattering force in the direction of propagation of the light. Both the Rayleigh and Mie approximations have been used to calculate evanescent trapping of particles [20, 34], but these approximations fail to describe the forces when the particles and waveguides are similar in dimension to the wavelength of the light used for trapping combined with when the evanescent fields are smaller in dimension than the size of the particles. Here we use a more rigorous approach based on the calculation of the Maxwell-Stress Tensor, which better represents the actual experiment. All of our simulations were conducted in 3D using a finite element method approach. For details on the numerical method refer to Yang and Erickson [33] where the same code was used to calculate the stable trapping regime in similar systems.

The optical forces acting on a particle can be calculated using the time-independent Maxwell stress tensor

$$\langle \mathbf{T}_M \rangle = \mathbf{D}\mathbf{E}^* + \mathbf{H}\mathbf{B}^* - \tfrac{1}{2}\left(\mathbf{D}\cdot\mathbf{E}^* + \mathbf{H}\cdot\mathbf{B}^*\right)\mathbf{I} \quad (1)$$

where $\mathbf{T}_M$ represents the Maxwell stress tensor, **E** is the electric field, **B** is the magnetic flux field, **D** is the electric displacement, **H** is the magnetic field, and **I** is the isotropic tensor. Since the transport processes of interest here occur on time scales much longer than the optical period, we use the time independent Maxwell stress tensor $\langle \mathbf{T}_M \rangle$. By integrating the time-independent Maxwell stress tensor on a surface enclosing the particle of interest, we can determine the total electromagnetic force acting on the system, $\mathbf{F}_{\mathbf{EM}}$, given by

#86071 - $15.00 USD Received 6 Aug 2007; revised 25 Sep 2007; accepted 27 Sep 2007; published 15 Oct 2007

$$\mathbf{F}_{EM} = \oint_S \left(\langle \mathbf{T}_M \rangle \cdot \mathbf{n} \right) dS \tag{2}$$

For simulation purposes, the light was assumed to be TM polarization. Particle sizes correspond to the size and type used in the experiments described in section 3. In our simulations a 10 nm gap was assumed between the bottom of the particle and the waveguide surface. This assumption is discussed in greater detail in section 6. We calculate the Maxwell stress tensor to evaluate the propagation and trapping forces directly.

Opposing the electromagnetic force is the hydrodynamic drag on the particle. In the low Reynolds number regime or interest here, this force is linearly proportional to particle velocity and is referred to as Stokesian drag. The terminal velocity of the particle on the waveguide is that which causes the drag and electromagnetic forces become equal. The drag force on the particle, $\mathbf{F}_D$, is described generally by

$$\mathbf{F}_D = \oint_S \left(\mathbf{T}_F \cdot \mathbf{n} \right) dS \tag{3}$$

where $\mathbf{T}_F$ is the fluid stress tensor, and $\mathbf{n}$ is the surface normal vector. In the most general sense, $\mathbf{F_D}$ from Eq. (1) is computed from a solution to the steady state Stokes flow (4a) and continuity Eqs. (4b).

$$\mu \nabla^2 \mathbf{v} - \nabla p = 0 \tag{4a}$$

$$\nabla \cdot \mathbf{v} = 0 \tag{4b}$$

where μ is the viscosity, $\mathbf{v}$ is the flow velocity vector and p is the pressure. Under these conditions the flow stress tensor is given by,

$$\mathbf{T}_F = -p\mathbf{I} + \mu\left(\nabla \mathbf{v} + \nabla \mathbf{v}^T \right) \tag{5}$$

where the final term in (3) is the rate of deformation tensor and $\mathbf{I}$ is the identity tensor.

The particle reaches its terminal optical transport velocity, $\mathbf{v_t}$, when these two forces ($\mathbf{F_{EM}}$ and $\mathbf{F_D}$) are equal. Generally speaking, for a system for a system exhibiting Stokesian drag the terminal velocity of the particle can be written as

$$\mathbf{v_t} = \frac{\mathbf{F_{EM}}}{C} \tag{6}$$

where C is a constant that contains the relationship between drag force and velocity. In the simplest case, the particle assumed to be moving through an infinite quiescent fluid, the solution to Eqs. (3) through (5) yields $C = 6\pi\mu a$, where a is the particle radius and μ is the viscosity. In the case of a particle near an infinite no-slip surface, which is more appropriate here, Faxen's Law [35] gives the constant term as,

$$C = \frac{6\pi a \mu}{\left[1 - \frac{9}{16}\left(\frac{a}{h}\right) + \frac{1}{8}\left(\frac{a}{h}\right)^3 - \frac{45}{256}\left(\frac{a}{h}\right)^4 - \frac{1}{16}\left(\frac{a}{h}\right)^5 \right]} \tag{7}$$

where h is the distance between the center of the particle and the surface. At smaller particle sizes, where the waveguide width is significantly larger than the particle diameter, Faxen's Law provides a good estimate for the constant term. For particle diameters of the same size

#86071 - $15.00 USD Received 6 Aug 2007; revised 25 Sep 2007; accepted 27 Sep 2007; published 15 Oct 2007

order or larger than the waveguide width, a numerical solution to Eq. (3) through (5) is required to determine the value of *C*.

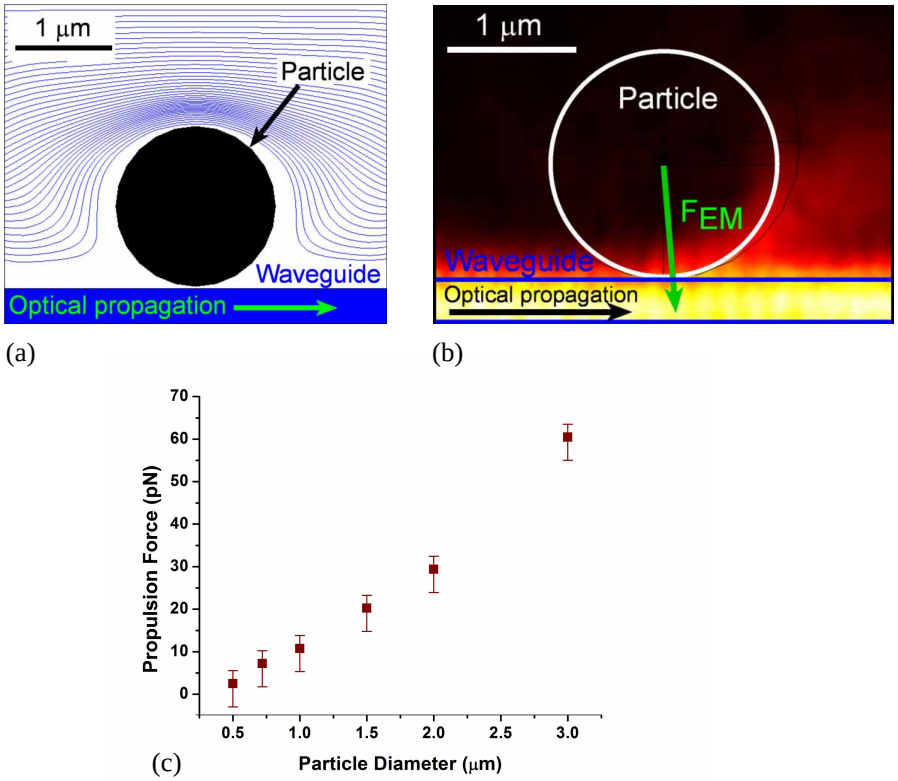

Fig. 5. Computed (a) flow streamlines and (b) electric field at the midplane of the waveguide. Particle in both cases is a 2.5 μm polystyrene sphere on a 560 nm tall and 2.8 μm wide SU-8 waveguide excited at 975 nm. Green arrow in (b) indicates the net direction of F_{EM}. (c) Plot of propulsion force per watt of input power as a function of particle size. Error bars indicate uncertainties in known particle size as reported by the manufacturer.

Figure 5 shows contour plots illustrative of the flow (a) of the particle and optical forces (b) acting on it. Figure 5c shows the propulsive force, computed using Eq. (2) above, as a function of particle size. The net trapping force acting on the particle serves to attract the particle towards the region of highest intensity and thus the simulations were conducted assuming that the particle was trapped in the center of the waveguide. The drag force on the particle was simulated by altering the frame of reference of the fluidic domain so that the microchannel walls were moving with respect to a non-moving particle (*i.e.* we applied a uniform slip boundary condition to the walls and Eq. (3) was used to compute the drag force as a function of velocity). To validate our flow simulations, we compared our computed drag forces to that obtained from Faxen's law [35] for a spherical particle near a surface. As expected good agreement was obtained for cases where the particle was much smaller than the width of the waveguide.

For a 500 nm diameter particle the simulations yielded a propagation force of 2.47 pN/W and gradient force of 24.79 pN/W. These values fall within the expected range when compared with previously reported values for lower index-contrast doped glass and more confining higher index-contrast silicon nitride waveguides by Gaugiran, *et al.* [24]. As can be seen in Fig. 5(c) over the range of particle sizes investigated here the computed dependence

#86071 - $15.00 USD Received 6 Aug 2007; revised 25 Sep 2007; accepted 27 Sep 2007; published 15 Oct 2007

of force on particle size was non-linear. Although the exact trend is difficult to extract without more data points below the 500nm diameter, over the range of interest here F_{EM} exhibited roughly a squared relationship with particle diameter. The simulated powers required for a 3 μm particle are also the correct magnitude when compared to the experimental obtained results, yielding a power dependent optical transport velocity of 691 μm/s/W for a 3μm particle compared with the measured value was 530 μm/s/W. The difference between the experimental and numerical results will be discussed in the next section.

6. Size specific particle separation

As expected, there also exists a significant dependence of particle optical transport velocity on size of the sphere. Various measurements were made to compare the transport behavior of several sizes of particles by performing alternating experiments between different pairs of particle sizes with different fluorescence emission wavelengths. The technique involved having two particles of different sizes transported in the channel at the same time, one with a green emission spectrum and one with a red emission spectrum. The relative optical transport velocity of the larger particle with respect to the smaller one could then be obtained under conditions in which the optical power at the trapping site could be ensured to be identical for both particles. This was repeated for a series of particle pair systems with decreasing diameters, each pair containing a particle that is the same size as one with the previous set. The average optical transport velocities were then normalized to that of the largest diameter particle (3μm) to yield the chromatographic relationship shown in Fig. 6. The importance of this technique is the removal of the dependence of optical power on transport velocity from the results. Each set of particle pair measurements were made simultaneously and therefore with the same waveguide power, ensuring that the true size dependent chromatographic behavior is reported. All measurements were performed using channels with same cross-sectional dimensions (5 μm x 100 μm) and, although not reflected in the final results, at input optical powers between 80 and 100 mW.

As shown in Fig. 6, smaller particles have slower optical transport velocities at the same guided power and the decrease in velocity with size is slightly sharper than that predicted by the numerical results (we normalize both the numerical and experimental results to the values obtained for the 3 μm particle). In both cases however a near linear trend is observed. This observation is consistent with the computed squared dependence of $\mathbf{F_{EM}}$ on particle diameter, as described in section 5, and the expected linear dependence of $\mathbf{F_D}$, from Eq. (7). It is important to note however that while this trend is valid over the range of interest here (where the particle diameter is significantly larger than the penetration depth of the evanescent field and of the same order as the width of the waveguide) firm conclusions about the transport behavior outside of this regime cannot be made.

The reason for this discrepancy between the numerical and experimental results is not yet clear. We do hypothesize that it could be the result of a variation in the stable position of the particle above the waveguide. As mentioned above, in our simulations we assumed the particles were a fixed distance of 10 nm above the waveguide. This was selected to be consistent with a strongly trapped particle subject to double layer repulsion between the similarly charged particle and waveguide. Given that the trapping forces vary strongly with particle size [32] and lift forces on the particle (induced by the strong flow shear near the surface as shown in Fig. 5(a) are also likely to depend on size, it is likely that the constant height assumption does not fully reflect the true physics of the system. Further analytical work is required to better understand this effect. In the measurements made here, we did not observe any obvious optical coupling from the evanescent field of the waveguide into a whispering gallery mode in the transported particles. It is not clear how such an effect would affect the particle transport, however, we expect that it may lead to some very localized deviations from the near linear relationship shown in Fig. 6.

#86071 - $15.00 USD Received 6 Aug 2007; revised 25 Sep 2007; accepted 27 Sep 2007; published 15 Oct 2007

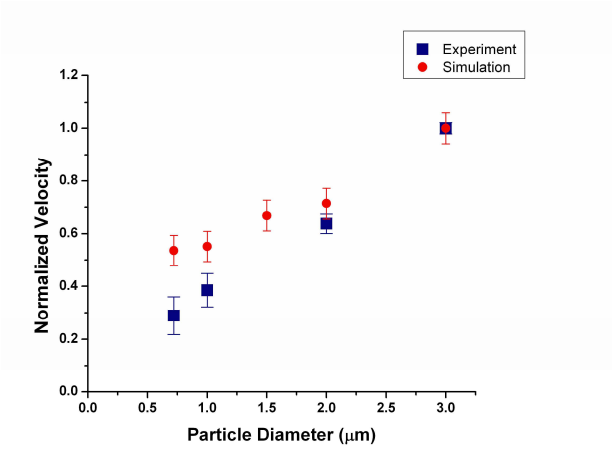

Fig. 6. Experimentally obtained and numerically computed relative particle terminal optical transport velocity as a function of particle diameter. Optical transport velocities measured perpendicular to the direction of the imposed pressure driven flow and thus represent only the effects of optical propulsion. Error bars on experimental results represent standard deviation of all measurements. Error bars on numerical simulations are representative of the uncertainty in known particle size (*i.e.* the upper bound and lower bound on the error bars are velocity values computed for upper and lower bounds of particle polydispersity as reported by the manufacturer).

7. Transport with waveguide bends

Optical trapping can be used as a form of transport in a microfluidic system in many different arrangements. For example, the situation above can be used to selectively trap and release particles from one flow position within a channel into another position to be separated using junctions further along the channel. One variation on this example is the use of angled or curved waveguides to collect and direct particles along specific flow lines. As shown in Fig. 7, particles entering in the lower half of the channel can be collected and propelled along one waveguide, and traveling at velocities greater than the surrounding non-trapped particles. At the same time, the size dependence of the velocity can be seen clearly in Fig. 7 as a trailing 3 μm particle is trapped after a 2 μm particle and then gains on the smaller particle until they collide. Analogous to the optical losses associated with tight bends in photonic systems, there may also exists a "critical bend radius" below which optofluidic transport on solid core waveguides may not be possible *i.e.* if the forward momentum of the transported particle exceeds the trapping stability [33] of the waveguide. Such a condition was not observed here.

#86071 - $15.00 USD Received 6 Aug 2007; revised 25 Sep 2007; accepted 27 Sep 2007; published 15 Oct 2007

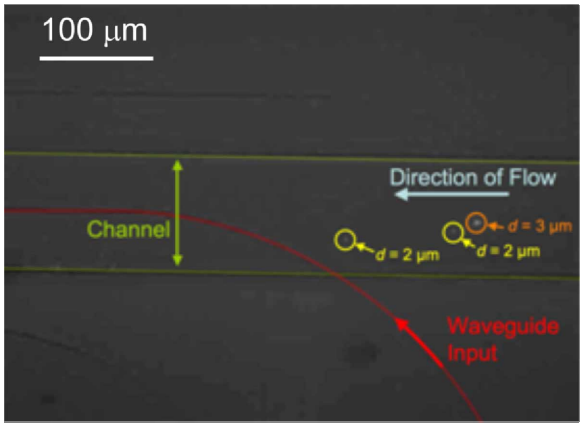

Fig. 7. (164 kB) Movie of 2 μm diameter particles trapped by a waveguide bend and overtaken by a trapped 3 μm diameter particle. The particles are all trapped and propelled along the same waveguide parallel to the channel flow.

Finally, the relative strength of the optical forces are clearly demonstrated in Fig. 8, where the particles are trapped by and propelled along a waveguide that is directed opposite to the direction of slow pressure-driven flow. As a particle approaches the waveguide from the left, it feels a trapping force that propels it back, following the curve of the waveguide bend.

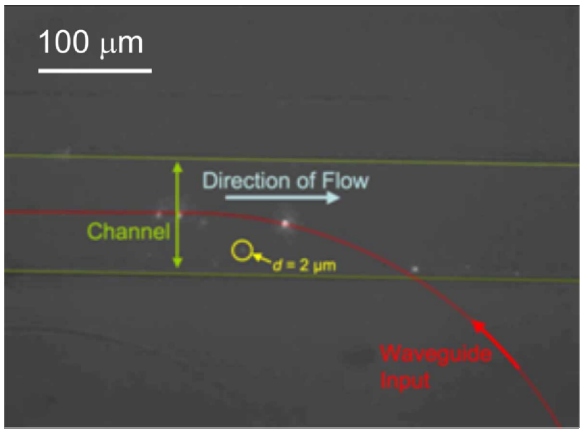

Fig. 8. (36 kB) Movie of 2 μm diameter particles trapped by a waveguide bend counter to the direction of pressure-driven flow.

8. Summary and Conclusions

In this article, we have demonstrated the use of optofluidic trapping and transport using planar photonic waveguides in a microfluidic channel. The evanescent field extending from the surface of optical waveguides is used to trap particles flowing over the waveguide and propel them perpendicularly to the pressure-driven flow. The velocity of the propagation along the waveguides was shown to be dependent on the total power coupled into the waveguide and the size of the particles. Velocities as high 28 μm/s were achieved using guided powers of 53.5 mW inside the waveguide.

#86071 - $15.00 USD Received 6 Aug 2007; revised 25 Sep 2007; accepted 27 Sep 2007; published 15 Oct 2007

The planar optofluidic architecture developed, comprising of SU-8 based photonic structures and PDMS fluidics on a fused silica substrate, represents a simple yet functional optical manipulation system for lab-on-chip applications. Although the focus of this paper is on transport characterization, we envision that such a system could find application in high stability particle trapping and sorting, but also for biomolecular detection by exploiting the strong light scattering observed when a particle interacts with the evanescent field.

Acknowledgments

This work was supported by the National Science Foundation under award numbers 0401222 and 0529045. This work was performed in part at the Cornell NanoScale Facility, a member of the National Nanotechnology Infrastructure Network, which is supported by the National Science Foundation (Grant ECS 03-35765).

#86071 - $15.00 USD Received 6 Aug 2007; revised 25 Sep 2007; accepted 27 Sep 2007; published 15 Oct 2007